# Electrochemically Oxidized Electronic and Ionic Conducting Nanostructured Block Copolymers for Lithium Battery Electrodes

**Shrayesh N. Patel,[†,‡,§] Anna E. Javier,[†,§] and Nitash P. Balsara[†,‡,§,*]**

[†]Environmental Energy Technologies Division, Lawrence Berkeley National Laboratory, Berkeley, California 94720, United States, [‡]Materials Sciences Division, Lawrence Berkeley National Laboratory, Berkeley, California 94720, United States, and [§]Department of Chemical and Biomolecular Engineering, University of California, Berkeley, California 94720, United States

**ABSTRACT** Block copolymers that can simultaneously conduct electronic and ionic charges on the nanometer length scale can serve as innovative conductive binder material for solid-state battery electrodes. The purpose of this work is to study the electronic charge transport of poly(3-hexylthiophene)-*b*-poly(ethylene oxide) (P3HT-PEO) copolymers electrochemically oxidized with lithium bis-(trifluoromethanesulfonyl) imide (LiTFSI) salt in the context of a lithium battery charge/discharge cycle. We use a solid-state three-terminal electrochemical cell that enables simultaneous conductivity measurements and control over electrochemical doping of P3HT. At low oxidation levels (ratio of moles of electrons removed to moles of 3-hexylthiophene moieties in the electrode), the electronic conductivity ($\sigma_{e,ox}$) increases from $10^{-7}$ S/cm to $10^{-4}$ S/cm. At high oxidation levels, $\sigma_{e,ox}$ approaches $10^{-2}$ S/cm. When P3HT-PEO is used as a conductive binder in a positive electrode with $LiFePO_4$ active material, P3HT is electrochemically active within the voltage window of a charge/discharge cycle. The electronic conductivity of the P3HT-PEO binder is in the $10^{-4}$ to $10^{-2}$ S/cm range over most of the potential window of the charge/discharge cycle. This allows for efficient electronic conduction, and observed charge/discharge capacities approach the theoretical limit of $LiFePO_4$. However, at the end of the discharge cycle, the electronic conductivity decreases sharply to $10^{-7}$ S/cm, which means the "conductive" binder is now electronically insulating. The ability of our conductive binder to switch between electronically conducting and insulating states in the positive electrode provides an unprecedented route for automatic overdischarge protection in rechargeable batteries.

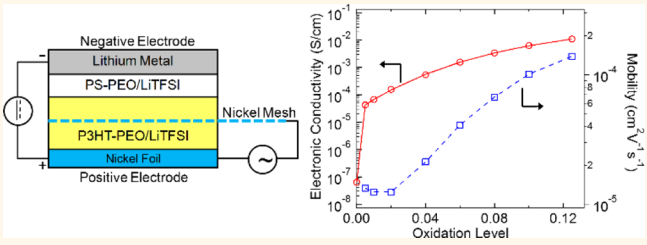


**KEYWORDS:** electrochemical oxidation · mixed conductor · electronic conductivity · ionic conductivity · conducting polymers · lithium battery · overdischarge protection

Materials with nanostructured conducting domains are essential for a wide range of applications related to alternative energy. Organic solar cells require nanoscale electron and hole-conducting domains to promote charge separation and extraction.[1] Active materials in battery and fuel cell electrodes, such as $LiFePO_4$, graphite, and platinum, are either electronic or ionic insulators.[2−4] Nanoscale electron- and ion-conducting domains are necessary for enabling redox reactions in these materials.[2−4] For example, a traditional porous lithium battery electrode consists of a redox-active material, carbon black for electronic conduction, and nonconductive binder that holds the particles in place. The pores are then backfilled with an organic electrolyte for ionic conduction. In some cases such as $LiFePO_4$, electronic and ionic conductivities are so low that the active materials must be in nanoparticle form, and addressing such particles requires the transport of both kinds of charges to occur on nanometer length scales. Materials such as block copolymers can self-assemble and form co-continuous nanoscale domains such as alternating lamellae, cylinders, or cubic gyroid phases.[5] Ionic conduction can, in principle, occur in one of the domains and electronic conduction in the other. In this study, which builds on the work in refs 30 and 33, poly(3-hexylthiophene)-*block*-poly(ethylene oxide) (P3HT-PEO) copolymers are

* Address correspondence to nbalsara@berkeley.edu.

Received for review April 15, 2013 and accepted June 11, 2013.

**Published online June 21, 2013**
10.1021/nn4018685

used to conduct both electronic and ionic charges. P3HT-PEO block copolymer molecules self-assemble on the nanometer length scale to yield P3HT domains that conduct electronic charges and PEO domains that conduct ionic charges. One can thus construct an electrode that consists of only the redox-active material and P3HT-PEO block copolymer.

P3HT is essentially an electronic insulator in its pristine state; it is formally a semiconductor with bulk electronic conductivity in the range $10^{-5}$–$10^{-8}$ S/cm.[6–12] It is likely that the higher range of the conductivity is due to the presence of small concentrations of contaminants. The electronic conductivity of conjugated polymers is increased by chemical doping, *i.e.*, the addition of chemical species such as ferric chloride, or by electrochemical doping, *i.e.*, the introduction of ionic species such as $PF_6^-$ under applied electrochemical potentials.[13–18] Seminal work of Chiang *et al.* showed that chemical doping increases the electronic conductivity of poly(acetylene) from $10^{-9}$ S/cm to $10^2$ S/cm after doping.[17] In the case of chemical doping, introduction of an oxidizing agent such $I_2$ (g) results in a spontaneous oxidation of the conjugated polymer. In the case of electrochemical doping, an applied potential drives the oxidation of the conjugated polymer. A formal positive charge (hole) created on the polymer backbone is compensated by diffusion of a dopant counterion into the polymer from the surrounding electrolyte. Electrochemical doping provides a unique avenue for designing the next generation of electrodes because it enables the possibility to turn redox reactions on and off reversibly through the control of applied potentials. This is in stark contrast to the traditional carbon additives used to conduct electrons in conventional battery and fuel cell electrodes, which have a fixed electronic conductivity.

The purpose of this study is to characterize the electronic transport in electrochemically doped P3HT-PEO block copolymers. We use a novel three-terminal cell that enables simultaneous conductivity measurements and control over electrochemical doping of P3HT. The results of our experiments provide further insight into the charge transport properties of P3HT-PEO block copolymers when used to conduct electronic and ionic charges in a lithium battery electrode. In particular, we demonstrate that the semiconducting properties of P3HT enable automatic overdischarge protection of the lithium battery.

The combination of conjugated polymers and electrolytes has been used in organic electrochemical transistors[19–22] and batteries (as the primary active material for electrodes[23–26] and for overcharge protection[27–29]). The traditional electrochemical oxidation of conjugated polymers consists of polymer films submerged or swollen with a liquid electrolyte.[16,27] In the case of solid-state organic electrochemical transistors, the conjugated polymer and polymer electrolyte are assembled as a bilayer. The conjugated polymer and polymer electrolyte are not chemically bonded across the interface between them. Our polymer is a unique electrochemical system in that the electrolyte is a solid polymer that is covalently bonded to the electronically conducting polymer. Block copolymer thermodynamics ensures microphase separation into co-continuous electronically conducting P3HT and ionically conducting PEO domains on the nanometer length scale. The characteristic periodic length scale for P3HT-PEO block copolymers used in this study is around 20 nm.[30] As a result, the dopant counterions have to diffuse only a few nanometers to compensate for the charged nature of the electrochemically oxidized P3HT chains. This can, in principle, enable rapid and efficient counterion diffusion during redox reactions.

**TABLE 1. Characteristics of Polymers Used in This Study**

| polymer name | $M_{n,P3HT}$[a] (kg/mol) | $M_{n,PEO}$[a] (kg/mol) | $\phi_{HT}$[b] (P3HT block) | $r_{HT}$[c][30] | $r_{EO}$[d][30] | morphology[30] |
|---|---|---|---|---|---|---|
| P3HT-PEO(9—2) | 9.0 | 2.0 | 0.81 | 0.017 | 0.065 | nanofibrillar |
| P3HT-PEO(6—2) | 6.0 | 2.0 | 0.74 | 0.016 | 0.072 | nanofibrillar |
| P3HT-PEO(5—4) | 5.0 | 4.2 | 0.53 | 0.0003 | 0.0849 | lamellar |

[a] $M_n$ = number-average molecular weight. [b] P3HT volume fraction. Calculated using P3HT density[31] of 1.10 g/mL and PEO density[32] of 1.06 g/mL. [c] LiTFSI salt concentration in P3HT phase. [d] LiTFSI salt concentration in PEO phase.

## RESULTS AND DISCUSSION

The characteristics of the P3HT-PEO block copolymers used in this study are summarized in Table 1. We examined mixtures of lithium bis(trifluoromethanesulfonyl) imide salt (LiTFSI) and P3HT-PEO block copolymers listed in Table 1. The LiTFSI salt concentration, $r_0$, is equal to 0.085 in all cases, where $r_0$ is the molar ratio of lithium ions to ethylene oxide moieties. All reported conductivity values were obtained at 90 °C, and reported potentials are relative to a $Li/Li^+$ reference electrode.

In our previous publication, we reported on the relationship between morphology and simultaneous electronic and ionic charge transport in P3HT-PEO/LiTFSI mixtures.[30] The same block copolymers were used in ref 30 and the current study. At 90 °C, the electronic conductivity of P3HT-PEO/LiTFSI mixtures, in the absence of applied potentials, ranged from $10^{-8}$ to $10^{-5}$ S/cm. The decoupled ionic conductivity was about $10^{-4}$ S/cm in all cases, a value that is reasonable for practical lithium battery applications. In addition, we showed a surprising increase in the electronic conductivity by simple chemical mixing of LiTFSI in the P3HT domains. This observation of increased conductivity was surprising, as LiTFSI does not have any of the characteristics of traditional chemical dopants; that is, it did not spontaneously oxidize P3HT. It was shown that the LiTFSI salt partitions between P3HT and PEO microphases. In Table 1, we present $r_{EO}$ and $r_{HT}$, the

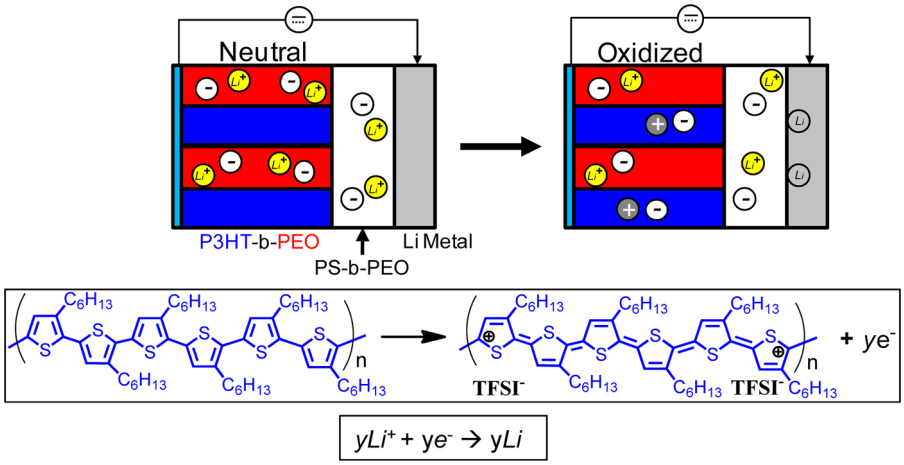


**Figure 1. Schematic of a two-terminal electrochemical cell. The positive electrode is a nanostructured P3HT-PEO block copolymer with LiTFSI at $r_0$ = 0.085. We show only four lamellar horizontal domains for simplicity. In reality, the block copolymer nanostructure would be composed of a large number of randomly oriented grains. The negative electrode is pure lithium metal, which also serves as the reference electrode. Electrons are transported between the positive and negative electrodes by an external circuit. Lithium ions are transported through the PS-PEO block copolymer electrolyte. During the oxidation reaction, an electron is removed from P3HT to generate a hole charge carrier on the polymer backbone. As a result, a $TFSI^-$ anion diffuses into the P3HT domain from the PEO domain. At the negative electrode, the electron produced at the P3HT-PEO electrode travels through the external circuit to react with a $Li^+$ to form Li metal. The $Li^+$ left behind by the transfer of the $TFSI^-$ anion in the $P3HT^+$ diffuses into the polymer electrolyte separator to compensate for the consumed $Li^+$ at the negative electrode.**

ratios of the moles of salt to the moles of ethylene oxide and 3-hexylthiophene moieties, respectively, as reported in ref 30. It is important to note that the conductivities reported in ref 30 correspond to neutral P3HT. In reality, the electronic conductivity can be further increased by electrochemically doping P3HT with LiTFSI.

A variety of electrochemical cells were used in this study. We begin by describing results obtained from a two-terminal electrochemical cell shown schematically in Figure 1. The negative electrode is lithium metal, which serves as the counter and reference electrode. The positive electrode is the P3HT-PEO/LiTFSI mixture. P3HT (blue) is the redox-active domain, and the LiTFSI primarily dissolved into the PEO domain (red) serves as the electrolyte in the positive electrode. Separating the two electrodes is a block copolymer electrolyte (polystyrene-*block*-polyethylene oxide, PS-PEO) layer with LiTFSI at $r_0$ = 0.085. This layer serves to transport lithium ions between the electrodes. The electrochemical cell configuration (Figure 1) is similar to our previously reported work on batteries with a lithium metal anode and lithium iron phosphate ($LiFePO_4$) cathode.[33] The difference is that the positive electrode does not contain $LiFePO_4$ redox-active particles. Removing the $LiFePO_4$ from the positive electrode enables the study of the electrochemical properties of P3HT-PEO block copolymers. The two half-reactions that occur in the electrochemical cell during the oxidation reaction are shown in Figure 1. One of the reactions is the oxidization of P3HT to $P3HT^+$, and the second reaction is the reduction of $Li^+$ to neutral Li. To oxidize P3HT, a positive current is applied to the cell; that is, an electron is removed from a 3-hexylthiophene moiety to generate a hole charge carrier (p-doping). This causes a $TFSI^-$ anion to diffuse from the PEO domain into the P3HT domain. In other words, the P3HT has been electrochemically doped with a $TFSI^-$ counterion. At the negative electrode, the electron produced at the P3HT electrode travels through the external circuit to react with a $Li^+$ ion to form Li metal. The $Li^+$ ion left behind by the transfer of the $TFSI^-$ anion into the $P3HT^+$ diffuses into the polymer electrolyte separator to compensate for the consumed $Li^+$ at the negative electrode. It is assumed that P3HT moieties are oxidized randomly as electrons are removed from the positive electrode, and it has been established that positive charges are separated by about six 3-hexylthiophene moieties.[34] The reactions in Figure 1 incorporate these assumptions.

A cyclic voltammetery experiment on the electrochemical cell depicted in Figure 1 indicated an onset oxidation of P3HT at 3.1 V and an oxidation peak at 3.6 V. The initial open circuit voltage (OCV), measured in all of our cells of the type in Figure 1, is 2.95 ± 0.05. This corresponds to the neutral state of P3HT. The oxidation levels of P3HT were controlled galvanostatically. A current density ($i$) of 0.17 mA/cm$^2$ was applied to the electrochemical cell for a specific amount of time ($t$). In Figure 2 we show a plot of the resulting cell potential ($E_{we}$) *vs* $t$ of a particular experiment on P3HT-PEO(6−2) where $t$ = 35 min. The oxidation level is denoted as $r_{ox}$, which is the ratio of the moles of electrons ($e^-$) removed in the galvanostatic experiment to the moles of the 3-hexylthiophene moieties in the positive electrode. The moles of $e^-$ removed are given by

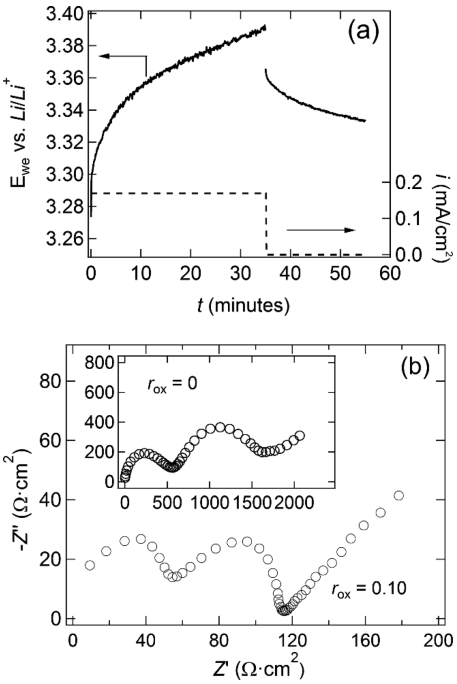


**Figure 2. (a) Characteristic cell voltage ($E_{we}$) *versus* time ($t$) profile (solid curve) and current density ($i$) *versus* $t$ (dashed lines) for the oxidation of P3HT-PEO(6−2) block copolymer with LiTFSI at $r_0$ = 0.085 using the two-terminal electrochemical cell. A current density of 0.17 mA/cm$^2$ is applied to the electrochemical cell until the desired oxidation level ($r_{ox}$) is reached. The cell is allowed to rest ($i$ = 0 mA/cm$^2$), after which the value of $E_{we}$ is taken as the oxidation potential ($E_{ox}$). (b) Nyquist impedance plot ($-Z''$ *vs* $Z'$) from 1 MHz to 100 mHz of a two-terminal electrochemical cell at 90 °C for $r_{ox}$ = 0 (inset) and $r_{ox}$ = 0.10. The positive electrode is P3HT-PEO(6−2) at $r_0$ = 0.085.**

$e^- = iAt/F$, where $A$ is the area of the sample (0.118 cm$^2$) and $F$ is Faraday's constant. We assume that the moles of $e^-$ removed equal the moles of TFSI$^-$ counterions in the oxidized P3HT microphases. After reaching the desired $r_{ox}$ value, the cell is allowed to rest until the $E_{we}$ "stabilizes" as shown in Figure 2a. In principle, the rest step allows for the dissipation of the electrode overpotentials and salt concentration gradients in the PS-PEO electrolyte and the P3HT-PEO electrode. It also allows for relaxation of inhomogeneous oxidation fronts that may have developed in the positive electrode. As can be seen in Figure 2a, even after a rest step of 25 min a steady decrease in $E_{we}$ of 0.001 V/min is observed. This may be the result of slow diffusion of ions across the electrode−electrolyte interface or uncontrolled side reactions. The value of $E_{we}$ is taken as the oxidation potential ($E_{ox}$), and the corresponding $r_{ox}$ is set by the galvanostatic step. Figure 2b shows the ac impedance spectroscopy measurements taken at $t$ = 0 before oxidation and after the rest step at $r_{ox}$ = 0.01. It is evident that the cell impedance decreases by about an order of magnitude in response to a small change in $r_{ox}$ from 0 to 0.01 (note the difference in the scales used for the $x$-axes in Figure 2b and the inset in Figure 2b). This is a clear sign that the P3HT chains are being oxidized.

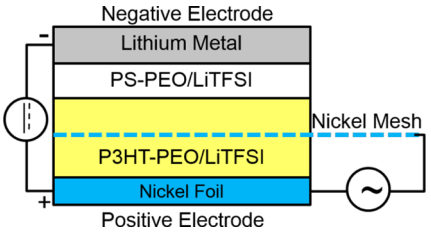


**Figure 3. Schematic of a three-terminal electrochemical cell that enables simultaneous conductivity measurements and control over electrochemical doping of P3HT. The nickel mesh (third terminal) is placed at the middle of the polymer layer of the positive electrode. The negative electrode is pure lithium metal, which also serves as the reference electrode. By applying a current between the positive and negative electrode, we can control the $r_{ox}$ value of the P3HT-PEO block copolymer. After reaching the desired $r_{ox}$ value, an ac impedance measurement is performed between the nickel foil of the positive electrode and the nickel mesh. This measurement allows us to directly quantify the conductivity of the oxidized P3HT-PEO block copolymer.**

Even though we see clear evidence of decreasing cell resistance in Figure 2b, the challenge lies in extracting the electronic resistance of the P3HT domains in the positive electrode. The cell pictured in Figure 1 cannot be used to address this challenge, as it contains several resistive components including the PS-PEO separator and the P3HT-PEO block copolymer, with concomitant interfacial and charge transfer resistances at each electrode.

In order to probe the electronic conductivity of the oxidized P3HT-PEO block copolymer directly, we modified the two-terminal cell (Figure 1) to include a nickel mesh in the P3HT-PEO positive electrode as shown in Figure 3. Following the procedure described above, a constant current is applied between the negative lithium metal electrode and the nickel foil of the positive electrode. After reaching the desired $r_{ox}$ value and allowing the cell to rest, ac impedance spectroscopy measurements are performed between the nickel foil and the nickel mesh both located in the P3HT-PEO electrode. This measurement quantifies the charge transport in the oxidized P3HT-PEO block copolymer. The $E_{ox}$ value was recorded after the rest step when stable impedance data were obtained (usually less than 30 min after the galvanostatic step).

In standard impedance measurements, one uses identical parallel plate electrodes to apply potentials and measure the resulting current. If edge effects are neglected, and the field lines are parallel to each other and perpendicular to the electrodes, the conductivity is calculated using eq 4 in the Experimental Methods section. In contrast, one of the electrodes used in the three-terminal cell is a mesh with 90% open area. In order to quantify the effect of using this mesh as an electrode, experiments were performed on a modified three-terminal cell as shown in Figure 4a. The cell in Figure 4a is symmetric with a P3HT-PEO/LiTFSI mixture sandwiched between two nickel foils and with a nickel

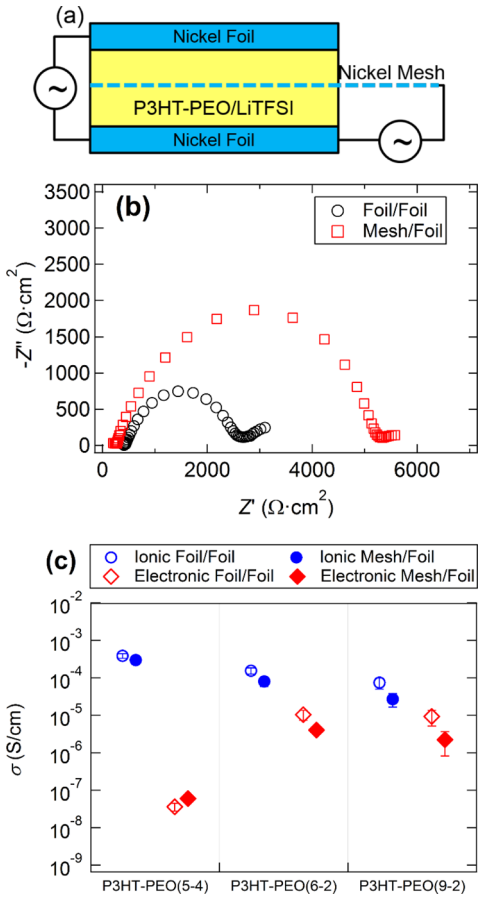


**Figure 4. (a) Schematic of a three-terminal conductivity cell used to quantify the effects of a nickel mesh electrode. (b) Representative Nyquist impedance plots ($-Z''$ *vs* $Z'$) for P3HT-PEO(6−2) at $r_0$ = 0.085 for a frequency range from 1 MHz to 10 mHz. Measurements are taken between the two nickel foil electrodes and between nickel foil and nickel mesh electrodes. (c) Electronic and ionic conductivity at 90 °C of the P3HT-PEO block copolymers at $r_0$ = 0.085 when measured between foil−foil electrodes and between foil−mesh electrodes.**

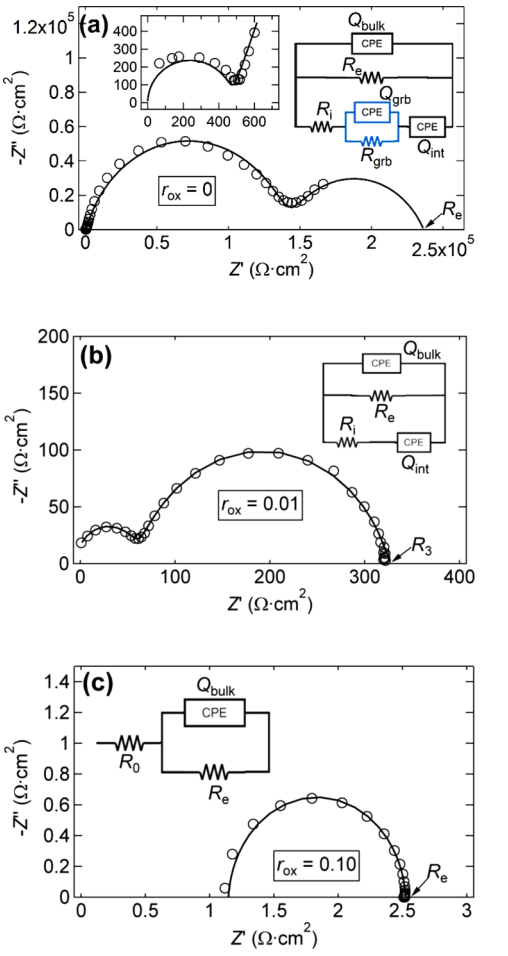


**Figure 5. (a) Characteristic Nyquist impedance plot ($-Z''$ *vs* $Z'$) at 90 °C for P3HT-PEO(6−2) at $r_{ox}$ = 0 with a frequency range of 1 MHz to 1 mHz. Fit parameters: $Q_{bulk} = 2.1 \times 10^{-10}$ F·s$^{a-1}$, $a_{bulk} = 1.0$, $Q_{int} = 1.60 \times 10^{-7}$ F·s$^{a-1}$, $a_{int} = 0.81$, $Q_{grb,fit} = 2.0 \times 10^{-7}$ F·s$^{a-1}$, $a_{grb} = 0.8$, $R_{i,fit} = 473\ \Omega\cdot cm^2$, $R_{grb,fit} = 3.4 \times 10^5\ \Omega\cdot cm^2$, $R_{e,fit} = 3.4 \times 10^5\ \Omega\cdot cm^2$. (b) Characteristic Nyquist impedance plot ($-Z''$ *vs* $Z'$) at 90 °C for P3HT-PEO(6−2) at $r_{ox}$ = 0.01 with a frequency range of 1 MHz to 100 Hz. Fit parameters: $Q_{bulk} = 1.51 \times 10^{-9}$ F·s$^{a-1}$, $a_{bulk} = 0.97$, $Q_{int} = 1.60 \times 10^{-7}$ F·s$^{a-1}$, $a_{int} = 0.81$, $R_{i,fit} = 130\ \Omega\cdot cm^2$, $R_{e,fit} = 310\ \Omega\cdot cm^2$. (c) Characteristic Nyquist impedance plot ($-Z''$ *vs* $Z'$) at 90 °C for P3HT-PEO(6−2) at $r_{ox}$ = 0.10 with a frequency range of 1 MHz to 55 Hz. Fit parameters: $Q_{bulk} = 1.7 \times 10^{-7}$ F·s$^{a-1}$, $a_{bulk} = 0.96$, $R_{0,fit} = 1.14\ \Omega\cdot cm^2$, $R_{e,fit} = 1.40\ \Omega\cdot cm^2$. These measurements are taken between the nickel foil and nickel mesh of the three-terminal electrochemical cell. The open circles represent experimental data, while the solid curve corresponds to the fit using the equivalent circuit shown in the inset.**

mesh in the middle. Impedance spectra were obtained in two independent experiments. In one case, the spectra were obtained using the two nickel foils as electrodes (foil−foil). In the other case, the spectra were obtained with one of the foils and a nickel mesh as the other electrode (mesh−foil). In Figure 4b we show impedance data obtained from a P3HT-PEO-(6−2)/LiTFSI mixture. The qualitative features seen in the foil−foil impedance data were similar to those seen in the mesh−foil impedance data. In both cases, the spectra were analyzed by methods described in ref 30 to give the electronic ($\sigma_e$) and ionic ($\sigma_i$) conductivities, using the same total polymer cross-sectional area (0.118 cm$^2$). The validity of $\sigma_e$ and $\sigma_i$ thus obtained may be questioned due to the large void fraction of nickel mesh. In Figure 4c, we show the values of $\sigma_e$ and $\sigma_i$ of the three P3HT-PEO/LiTFSI samples (Table 1). The values of $\sigma_e$ and $\sigma_i$ obtained in the foil−foil experiments reported in Figure 4c are within experimental error of those reported in ref 30. This is reasonable, as one does not expect the presence of the nickel mesh in the sample to have a measurable effect on charge transport in P3HT-PEO. The values of $\sigma_i$ obtained from the foil−foil and mesh−foil configuration are within experimental error. The $\sigma_e$ of P3HT-PEO(5−4) and P3HT-PEO(6−2) are also within experimental error. Only $\sigma_e$ of P3HT-PEO(9−2) from the mesh−foil experiment is significantly different from the foil−foil experiment. With the exception of $\sigma_e$ of P3HT-PEO(5−4), which is near the lower limit of the instrumental resolution, values of $\sigma_e$ obtained from the mesh−foil are lower than the

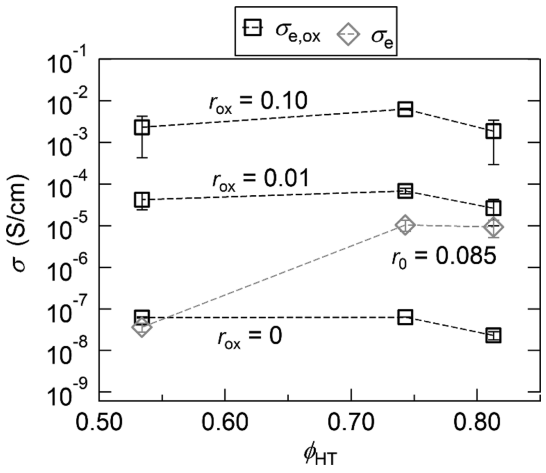


**Figure 6. Electronic conductivity of the oxidized P3HT-PEO block copolymers ($\sigma_{e,ox}$) at 90 °C as a function of the P3HT volume fraction ($\phi_{HT}$) for $r_{ox}$ values of 0, 0.01, and 0.10. The $\phi_{HT}$ values for the three block copolymers are given in Table 1. The diamond markers correspond to the electronic conductivity of the unoxidized P3HT-PEO block copolymers ($\sigma_e$) when only considering the chemical mixing of LiTFSI at $r_0$ = 0.085 and determined using a two-terminal conductivity cell. The dashed lines are guides for the eye.**

foil−foil experiments. One may thus consider $\sigma_e$ obtained from the mesh−foil experiments to be lower limits of the actual electronic conductivity. It is evident from Figure 4c that one cannot account for the mesh electrode using a multiplicative correction factor that applies to all samples. For consistency, we report conductivity values with the mesh−polymer−foil configuration without any corrections.

In Figure 5 we show Nyquist impedance plots of P3HT-PEO(6−2) obtained using the three-terminal electrochemical cell at $r_{ox}$ values of 0, 0.01, and 0.10. At $r_{ox}$ = 0, the Nyquist plot contains three semicircles. A small increase in $r_{ox}$ to 0.01 results in a Nyquist plot with two semicircles. At $r_{ox}$ 0.10, the Nyquist plot contains only one semicircle. The methodology to obtain the electronic and ionic conductivities of P3HT-PEO/LiTFSI mixtures from Nyquist plots is discussed at length in ref 30. Regardless of the number of Nyquist semicircles, the electronic resistance, $R_e$, is given by the intersection of the lowest frequency semicircle with the real axis. The curves through the data in Figure 5 are fits using the equivalent circuits in the insets of each figure. The method used to obtain the fit is described in ref 30. The electronic conductivities of the oxidized polymers ($\sigma_{e,ox}$) were calculated from $R_e$ values thus obtained using eq 4 described in the Experimental Methods section.

In Figure 6, we present $\sigma_{e,ox}$ of electrochemically oxidized P3HT-PEO block copolymers at $r_{ox}$ = 0, 0.01, and 0.10. At $r_{ox}$ = 0, $\sigma_{e,ox}$ is between $10^{-7}$ and $10^{-8}$ S/cm for all three polymers. It is evident in Figure 6 that the electronic conductivities of electrochemically oxidized P3HT-PEO block copolymers are weak functions of P3HT volume fraction ($\phi_{HT}$), where increasing $r_{ox}$ from 0 to 0.01 results in a 1000-fold increase in $\sigma_{e,ox}$. One might have mistakenly inferred a 10 fold increase in $\sigma_{e,ox}$ based on data obtained using the 2-terminal cell shown in Figure 2b. Further increase in $r_{ox}$ from 0.01 to 0.10 results in a 100-fold increase in $\sigma_{e,ox}$.

Also shown in Figure 6 is the electronic conductivity of unoxidized P3HT-PEO block copolymers ($\sigma_e$) obtained using a two-terminal conductivity cell with nickel foil electrodes. Note that both two-terminal and three-terminal experiments probe unoxidized P3HT-PEO block copolymers at $r_0$ = 0.085. In spite of this, it is evident in Figure 6 that $\sigma_{e,ox}$ at $r_{ox}$ = 0 is about 3 orders of magnitude lower than $\sigma_e$ for both P3HT-PEO(9−2) and P3HT-PEO(6−2). It was shown in ref 30 that the high values of $\sigma_e$ in P3HT-PEO(9−2) and P3HT-PEO-(6−2) are due to partitioning of salt into the P3HT microphase. In contrast, the salt is located exclusively in the PEO microphase in the case of P3HT-PEO(5−4). We propose that the higher chemical potential of LiTFSI for P3HT-PEO block copolymers with a PEO molecular weight of 2 kg/mol drives the LiTFSI into the P3HT-rich microphase. In the two-terminal conductivity cell, the LiTFSI chemical potential can be decreased only by partitioning into the P3HT microphase. In the three-terminal electrochemical cell, however, the LiTFSI chemical potential can be decreased by partitioning into the PS-PEO electrolyte layer where the PEO molecular weight is 67.6 kg/mol. We thus conclude that the electronic conductivities of all three P3HT-PEO block copolymers measured in the three-terminal electrochemical cell and that of P3HT-PEO-(5−4) measured in the cell with two-terminal conductivity correspond to a pure P3HT microphase with no added LiTFSI. There are two potential reasons for the increase in LiTFSI chemical potential in P3HT-PEO(9−2) and P3HT-PEO(6−2) relative to P3HT-PEO(5−4): (1) P3HT-PEO(9−2) and (6−2) have a nanofibrillar morphology, while P3HT-PEO(5−4) has a lamellar morphology. Disruption of the PEO domains in the presence of the nanofibrillar morphology may increase the LiTFSI chemical potential. (2) The interfacial area per unit volume between ionically conducting and nonionically conducting microdomains (either P3HT or PS) is expected to increase with decreasing PEO block molecular weight. The increased contact between salt and P3HT monomers due to this effect will also increase the LiTFSI chemical potential in P3HT-PEO(9−2) and (6−2).

Figure 7 shows conductivity data obtained in the three-terminal electrochemical cells as the P3HT-PEO block copolymers are cycled between oxidized and reduced states. A cycle consisted of oxidation in two steps, from $r_{ox}$ = 0 to $r_{ox}$ = 0.01 and from $r_{ox}$ = 0.01 to $r_{ox}$ = 0.10, using the galvanostatic oxidation protocol described above. Each step took about one hour to execute. In the reduction step, the electrons were added to the P3HT-containing electrode until the voltage cutoff of 2.5 V was reached, and the cell was

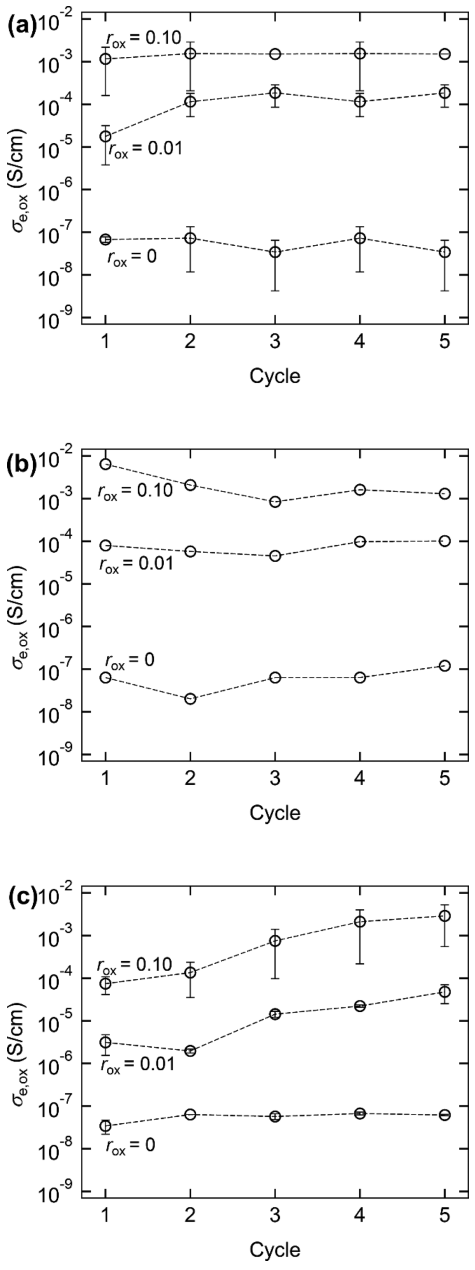


**Figure 7. Electronic conductivity of the oxidized (a) P3HT-PEO(9−2), (b) P3HT-PEO(6−2), and (c) P3HT-PEO(5−4) block copolymers at 90 °C for $r_{ox}$ values of 0. 0.01, and 0.10 for five oxidation/reduction cycles. A cycle consisted of oxidation from $r_{ox}$ = 0 to $r_{ox}$ = 0.10 and then reduction back to a neutral state of $r_{ox}$ = 0, which corresponds to the start of the next cycle. The dashed lines are guides for the eye.**

allowed rest until a stable value of conductivity was obtained. Full reduction of the P3HT chains back to the neutral state took several such steps and typically required three days. In the oxidation step, the $TFSI^-$ anion diffuses through the PEO microphase into the P3HT microphase. In the reduction step, the $TFSI^-$ anion diffuses through the P3HT microphase into the PEO microphase. Our experiments suggest that the diffusion of the $TFSI^-$ anion through P3HT is much slower than through PEO. It is likely that this is due to the crystalline nature of the P3HT domains in the presence and absence of LiTFSI.[30] It is evident in Figure 7 that the dependence of $\sigma_{e,ox}$ of P3HT-PEO(9−2) and P3HT-PEO(6−2) on $r_{ox}$ is independent of cycle number. In the case of P3HT-PEO(5−4), $\sigma_{e,ox}$ increases with each cycle at both $r_{ox}$ values of 0.01 and 0.10. The largest increase occurs between cycle 2 and 3. The data obtained in cycles 4 and 5 are almost within experimental error but show signs of stabilizing after subsequent cycling. Even though $\sigma_{e,ox}$ at $r_{ox}$ = 0.01 and 0.10 generally increases with cycle number, the baseline conductivity obtained at $r_{ox}$ = 0 is within experimental error in all cases.

Small-angle X-ray scattering (SAXS) experiments were performed on the oxidized samples at $r_{ox}$ = 0.10 after the fifth cycle. Figure 8a shows the SAXS intensity, *I*, *versus* magnitude of the scattering vector, *q*, of P3HT-PEO(5−4) at $r_{ox}$ = 0 and 0.10. The SAXS profile of P3HT-PEO(5−4) at $r_{ox}$ = 0 shows a primary peak at $q = q^* = 0.31$ $nm^{-1}$ and a higher order peak at $2q^*$, indicating the presence of a lamellar structure with a domain spacing $d = 20.3$ nm ($d = 2\pi/q^*$). At $r_{ox}$ = 0.10, the SAXS profile of P3HT-PEO(5−4) shows only a primary peak at $q^* = 0.28$ $nm^{-1}$ corresponding to a domain of $d$ = 22.4 nm. It is clear from the scattering profile that oxidation of P3HT results in the reduction of long-range order, as indicated by the loss of the second-order peak.[35] The SAXS profile of P3HT-PEO(9−2) at $r_{ox}$ = 0 shows a broad peak at $q^* = 0.31$ $nm^{-1}$ corresponding to $d$ = 20.3 nm (Figure 8b). Subtle shoulders are seen at higher values of *q*. These are signatures of the nanofibrillar morphology typically seen with P3HT-containing block copolymers. At $r_{ox}$ = 0.10, the SAXS profile of P3HT-PEO(9−2) also shows the nanofibrillar morphology with a broad peak at $q^* = 0.29$ $nm^{-1}$ corresponding to $d$ = 22 nm. Unlike P3HT-PEO(5−4), no significant change in morphology is seen upon oxidation of P3HT-PEO(9−2). In both Figure 8a and b, we see that *d* increases with oxidation [*d* increases 10% in P3HT-PEO(5−4) and 6% for P3HT-PEO(9−2)]. The transformation of the P3HT backbone from the benzenoid-like structure to the quinoid-like structure results in an increase in the persistence length of the polymer.[36] We propose the observed increase in *d* upon oxidation is due to this effect.

The important parameters that described the effects of electrochemical oxidation on electronic conductivity of P3HT-PEO block copolymers are $\sigma_{e,ox}$, $r_{ox}$, and $E_{ox}$. The relationships between these parameters are shown in Figure 9. Figure 9a shows $\sigma_{e,ox}$ as a function of $r_{ox}$ for the three P3HT-PEO block copolymers. The dependence of $\sigma_{e,ox}$ on $r_{ox}$ is similar for all three block copolymers. The data appear to fall into two regimes. The first regime encompasses low oxidation levels, and it is found that $\sigma_{e,ox}$ increases by approximately 3 orders of magnitude when $r_{ox}$ increases from 0 to 0.005. In the second regime, further increase of $r_{ox}$ from 0.005 to about 0.10 results in a more modest increase in $\sigma_{e,ox}$, with some evidence of saturation at $\sigma_{e,ox}$ of $10^{-2}$ S/cm at

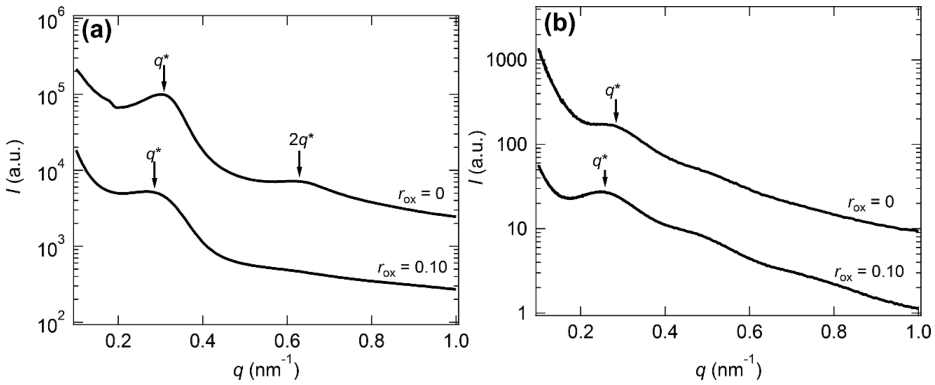


**Figure 8. (a) SAXS profile of P3HT-PEO(5−4) at 90 °C for $r_{ox}$ = 0 and 0.01 indicating the presence of microphase separation. A lamellar morphology is seen at $r_{ox}$ = 0, while there is a decrease in long-range order after oxidation to $r_{ox}$ = 0.10. (b) SAXS profile of P3HT-PEO(9−2) at 90 °C for $r_{ox}$ = 0 and 0.01 indicating a microphase-separated structure (nanofibrillar).**

high $r_{ox}$ values. The trends seen in Figure 9a are consistent with previously reported behavior of chemically oxidized conjugated polymers.[17] The highest $r_{ox}$ values attainable, 0.10, 0.125, and 0.150 for P3HT-PEO(9−2), P3HT-PEO(6−2), and P3HT-PEO(5−4), respectively, increase with decreasing molecular weight of the P3HT block. Chen *et al*. report $r_{ox}$ values as high as 0.30 for poly(3-butylthiophene) immersed in $LiPF_6$-containing liquid electrolyte and corresponding bulk electronic conductivities as high as 0.1 S/cm. However, Ciprelli *et al*. found considerably lower values of $r_{ox}$ when poly(3-octylthiophene) was chemically doped with a salt containing the $TFSI^-$ anion.[37] In Figure 9b, we show the relationship between $r_{ox}$ and $E_{ox}$, which has a power law relationship (the solid curves are power law fits to the data points). Even though each block copolymer has a different highest attainable $r_{ox}$, the corresponding highest attainable $E_{ox}$ is about 3.6 V in all cases. In Figure 9c, we show the relationship between $E_{ox}$ and $\sigma_{e,ox}$. It is clear that $\log(\sigma_{e,ox})$ increases linearly with $E_{ox}$.

Figure 10 shows the hole mobility ($\mu_{ox}$) of electrochemically oxidized P3HT-PEO block copolymer as a function of $r_{ox}$. The mobilities were calculated from the relation $\mu_{ox} = \sigma_{e,ox}/ne$, where $n$ is the charge carrier density ($cm^{-3}$) and $e$ is the elementary charge. The value of $n$ is calculated from $r_{ox}$; $n = r_{ox}N_{av}\rho_{P3HT}/M_{0,HT}$, where $N_{av}$ is Avogrado's number, $\rho_{P3HT}$ is the density of P3HT, and $M_0$ is molar mass of the 3-hexylthiophene repeat unit. Note that both $\sigma_{e,ox}$ and $n$ are functions of electrochemical potential of the polymer (Figure 9). The $\mu_{ox}$ *vs* $r_{ox}$ data in Figure 10 appear to fall into two regimes. For $r_{ox}$ values less than 0.02, $\mu_{ox}$ is a weak function of $r_{ox}$. Above $r_{ox}$ = 0.02, $\mu_{ox}$ increases linearly nearly 1 order of magnitude as $r_{ox}$ is increased to about 0.10. In this regime, hole mobility is independent of block copolymer composition or the chain length of the P3HT block. The data in Figure 10 are qualitatively similar to those obtained from electrochemically doped P3HT homopolymer in the presence of a liquid electrolyte.[38−40] Arkhipov *et al*. explained the observed trend in mobility assuming a transport model that accounts for Coulombic interactions between the holes and counterions. An important parameter in the model is the reciprocal localization radius ($\gamma$), which was varied to obtain agreement between theory and experiment. At low $r_{ox}$ values, the holes generated are trapped by the attractive Coulomb potentials of the $TFSI^-$ anion (Coulomb traps). As a result, the mobility of the holes is suppressed. The several orders of magnitude increase in $\sigma_{e,ox}$ (Figure 9a) at low $r_{ox}$ is entirely from the increase in charge carrier density. As $r_{ox}$ increases, the distance between the holes (and TFSI anions) decreases, which results in the overlap of the Coulomb trap potential energy wells. This reduces the activation barrier for hole transport and enhances mobility. Remarkably, the data in Figure 10 are in quantitative agreement with Arkhipov *et al*. with $\gamma = 3\ nm^{-1}$; that is, $\mu_{ox}$ increases from $10^{-5}$ to $10^{-4}\ cm^2 \cdot V^{-1} \cdot s^{-1}$ as $r_{ox}$ is increased by a factor of 10 (Figure 4 in ref 40). A difference between our data and the model is that in the model the linear regime starts at $r_{ox} \approx 0.1$, while in our experiments this regime starts at $r_{ox} \approx 0.01$.

Figure 11 shows the schematic of a battery with a lithium metal negative electrode and a $LiFePO_4$ positive electrode. The $LiFePO_4$ particles (active material) are dispersed in a P3HT-PEO(6−2)/LiTFSI mixture. Separating the two electrodes is a PS-PEO block copolymer electrolyte layer with LiTFSI at $r_0$ = 0.085. The properties of this battery were reported in ref 33, where it was shown that the P3HT-PEO(6−2)/LiTFSI serves as an electronically and ionically conducting binder and that the charge/discharge specific capacity of the positive electrode approaches the theoretical value of $LiFePO_4$ (170 mAh/g).[33] The theoretical specific capacity for P3HT is 161 mAh/g. We focus on a single charge/discharge cycle to elucidate the changes in the electronic conductivity and oxidation level of P3HT during a battery cycle, as shown in Figure 12a. The voltage of the battery ($E_{we}$ *vs* $Li/Li^+$) is initially at its equilibrium OCV of 3.41 V. The battery is then charged at a constant $i$ of 0.02 $mA/cm^2$ until $E_{we}$ reaches 3.8 V. $E_{we}$ is held at 3.8 V until $i$ decreased to 10% of the

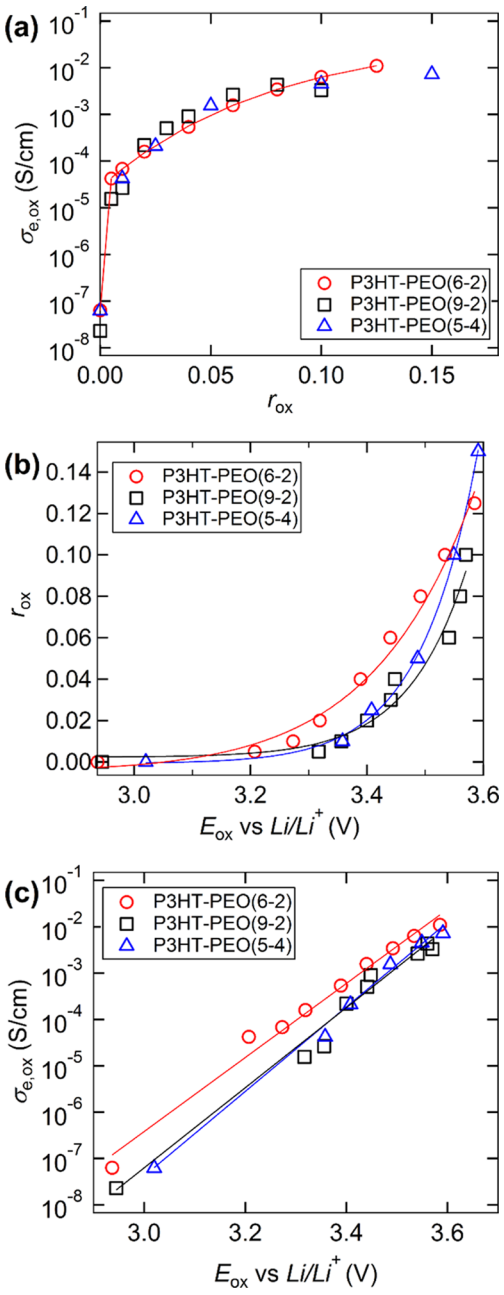


**Figure 9. (a) Electronic conductivity of the oxidized P3HT-PEO block copolymers ($\sigma_{e,ox}$) as a function of oxidation level ($r_{ox}$). The solid line corresponds to a line fit between $r$ = 0 and 0.005. The solid curve corresponds to a fit using $\log(\sigma_{e,ox}) = a - b(10^{c*rox/d})$ from $r_{ox}$ = 0.005 to 0.125, where $a = -1.32$, $b = 3.24$, $c = 1120$, and $d = 86.2$. Fit is given only for P3HT-PEO(6−2) for clarity. (b) Relationship between $r_{ox}$ and $E_{ox}$ for the P3HT-PEO block copolymers. Open circles are the experimental data, and the solids curves are power law fits. Fit parameters using the equation $r_{ox} = a + b(E_{ox})^c$: $a = -4.97 \times 10^{-3}$, $b = 8.08 \times 10^{-13}$, and $c = 20.6$ for P3HT-PEO(6−2), $a = 2.28 \times 10^{-3}$, $b = 3.25 \times 10^{-21}$, and $c = 35.2$ for P3HT-PEO(9−2), and $a = -7.54 \times 10^{-4}$, $b = 1.31 \times 10^{-21}$, and $c = 36.1$ for P3HT-PEO(5−4). (c) Electronic conductivity of the oxidized P3HT-PEO block copolymers as a function of cell potential ($E_{ox}$ *vs* $Li/Li^+$). Open circles are the experimental data, and the solid lines are linear (log-scale) fits. Fit parameters using the equation $\log(\sigma_{e,ox}) = a + b(E_{ox})$: $a = -30.4$ and $b = 7.99$ for P3HT-PEO(6−2), $a = -33.1$ and $b = 8.63$ for P3HT-PEO(9−2), and $a = -34.7$ and $b = 9.11$ for P3HT-PEO(5−4). All conductivity data are at 90 °C.**

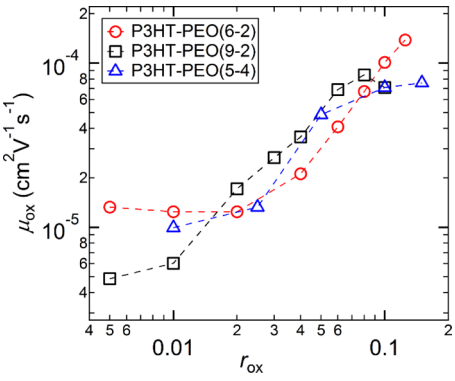


**Figure 10. Hole mobility ($\mu_{ox}$) of electrochemically oxidized P3HT-PEO block copolymers as a function of oxidation level ($r_{ox}$). The mobilities were calculated from the relation $\mu_{ox} = \sigma_{e,ox}/ne$, where $n$ (related to $r_{ox}$) is the charge carrier density ($cm^{-3}$) and $e$ is the elementary charge. The dashed lines are guides for the eye.**

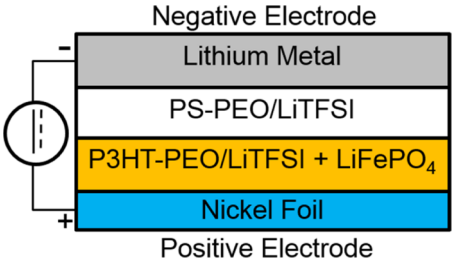


**Figure 11. Schematic of a battery cell with a positive electrode comprising $LiFePO_4$ active material, LiTFSI, and P3HT-PEO binder. The negative electrode is pure lithium metal, which also serves as the reference electrode. In between the positive and negative electrode is a PS-PEO/LiTFSI electrolyte layer.**

original value, which completes the charging step. After a rest step of 60 min, the battery is discharged at a constant $i$ of −0.02 mA/cm$^2$ until $E_{we}$ reaches 2.5 V. After another rest step, $E_{we}$ increases until it returns to the equilibrium OCV value of 3.41 V. This completes the charge/discharge cycle. Note that the $E_{we}$ values found in the battery (Figure 12a) overlap with the range of $E_{ox}$ values given in Figure 9c. Interestingly, the voltage window where P3HT is electrochemically active is within the voltage range of the battery charge/discharge cycle. The reversible redox reactions occurring in the battery are

$$x\mathrm{LiFePO_4} \underset{\text{discharge}}{\overset{\text{charge}}{\rightleftharpoons}} x\mathrm{FePO_4} + xe^- + x\mathrm{Li^+} \quad (1)$$

$$y\mathrm{P3HT} \underset{\text{discharge}}{\overset{\text{charge}}{\rightleftharpoons}} y\mathrm{P3HT^+} + ye^- \quad (2)$$

$$(x+y)\mathrm{Li^+} + (x+y)e^- \underset{\text{discharge}}{\overset{\text{charge}}{\rightleftharpoons}} (x+y)\mathrm{Li} \quad (3)$$

The forward reaction corresponds to the charging step, while the reverse reaction corresponds to the discharging step. Reactions 1 and 2 occur in the positive electrode, while reaction 3 occurs in the negative electrode. In Figure 12b, we show the time dependence

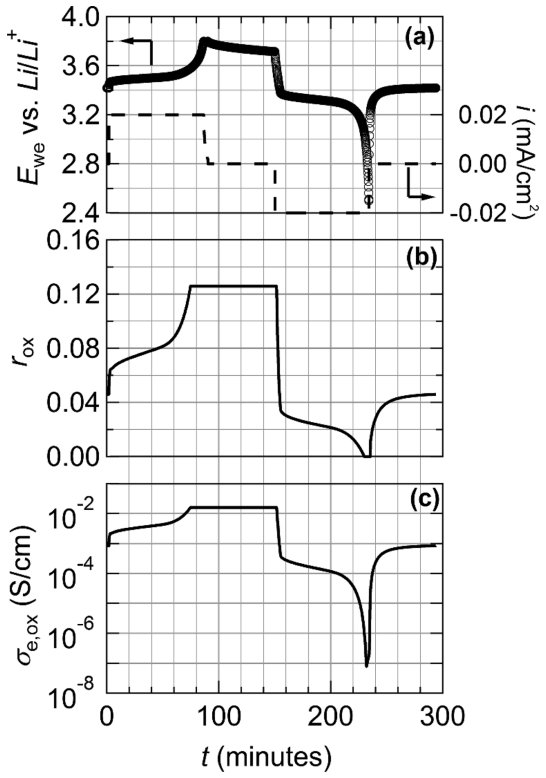


**Figure 12. (a) Cell potential ($E_{we}$ *vs* Li/Li$^+$) *vs* time ($t$) curve corresponding to a characteristic charge/discharge profile for a battery cell composed of a lithium anode, solid polymer electrolyte, and a $LiFePO_4$ positive electrode with P3HT-PEO(6−2) conductive binder. (b) Oxidation level ($r_{ox}$) for the charge/discharge profile using the relationship between $E_{ox}$ and $r_{ox}$ given in Figure 9b. (c) Oxidized electronic conductivity ($\sigma_{e,ox}$) for the charge/discharge profile using the relationship between $E_{ox}$ and $\sigma_{e,ox}$ given in Figure 9c.**

of $r_{ox}$ during the charge/discharge cycle. This curve was calculated from the power law fit through P3HT-PEO-(6−2) data in Figure 9b. During the charging step, $r_{ox}$ was assumed to follow the power law until the maximum $r_{ox}$ value was reached. During this time, we assumed that both $LiFePO_4$ and P3HT are oxidized. In the remainder of the charging step, we assume that all of the oxidation occurs in the $LiFePO_4$ particles. We assume that $r_{ox}$ remains constant during the rest step and follows the power law in the subsequent discharging and rest steps. At a $r_{ox}$ value of 0.125, P3HT contributes only about 7% to the total capacity of the battery (far from the theoretical specific capacity of P3HT).

In Figure 12c, we show the time dependence of $\sigma_{e,ox}$ during the charge/discharge cycle obtained using the fit through the P3HT-PEO(6−2) data shown in Figure 9c. It is evident that the conductivity of our binder is relatively high, in the $10^{-3}$ to $10^{-2}$ S/cm range, during charging. This value is significantly higher than the ionic conductivity of the P3HT-PEO(6−2)/LiTFSI mixture ($10^{-4}$ S/cm) reported in ref 30. This is important for enabling the redox reactions 1 to 3 because they involve equal moles of ions and electronic charges. It is, perhaps, not surprising that high electronic conductivity is obtained during charging because the P3HT chains are being oxidized during this step. During most of the discharge step, electronic conductivity is above $10^{-4}$ S/cm. This may seem surprising because P3HT is being reduced during this step. Electronic conductivity during the discharge step is enabled entirely due to the potential of 3.3 V imposed on the positive electrode by the $FePO_4$ particles. As the discharge step approaches completion and $E_{we}$ decreases to 2.5 V (Figure 12b), $\sigma_{e,ox}$ plummets to below $10^{-7}$ S/cm. In other words, our "conductive" binder is essentially an electronic insulator toward the end of the discharge cycle. This provides a unique route for overdischarge protection as the battery has been essentially "shut off" to further discharge. After the discharge cycle, the battery returns back to an equilibrium OCV value of 3.41 V, where $\sigma_{e,ox} = 1 \times 10^{-3}$ S/cm, indicating that the binder returns to the electronically conducting state.

It is important to have overdischarge and overcharge protection in a battery in order to improve the safety and cycle life of the battery. In a conventional battery pack, overdischarge and overcharge protection is accomplished using external circuitry. Unfortunately, the use of external circuitry adds significant weight, adds to the cost, and complicates battery pack design. Therefore, it is advantageous to incorporate the overdischarge or overcharge protection capabilities within the chemistry of the battery cell, thus simplifying the battery pack design and reducing the cost. In some experimental battery cells, redox shuttles are used to enable overcharge and overdischarge protection within a battery cell.[41] In an interesting experiment, Chen *et al.* lined the pores of a conventional battery separator with P3BT. Under the conditions where the cells were fully charged, the P3BT lining became electronically conducting and the additional electrons were directly shuttled from the negative to the positive electrode.[28,29] The charging process is thus interrupted. Alternatively, incorporating a semiconducting binder in one of the electrodes (as we do in this study) provides a radically new approach for enabling overdischarge and overcharge protection. In principle, a semiconducting binder in the positive electrode could provide overdischarge protection, as shown in this study, while a semiconducting binder in the negative electrode could provide overcharge protection.

## CONCLUSIONS

We have characterized electronic charge transport in P3HT-PEO block copolymers as a function of electrochemical doping. A novel three-terminal electrochemical cell that enables simultaneous conductivity measurements and control over electrochemical doping of P3HT in a solid-state system was developed. The electronic conductivity ($\sigma_{e,ox}$) of the P3HT-PEO block copolymers is measured as a function of oxidation level, $r_{ox}$, and

oxidation voltage, $E_{ox}$. At low $r_{ox}$ values below 0.01, $\sigma_{e,ox}$ increases from $10^{-8}$ S/cm to nearly $10^{-4}$ S/cm. At $r_{ox}$ values near the highest attainable oxidation levels, $\sigma_{e,ox}$ approaches $10^{-2}$ S/cm. The three-terminal cell enables determination of the mobility of electronic charges in P3HT-PEO copolymers, as it enables measurement of conductivity in the presence of a known concentration of charge carriers. Finally, we show the effect of the presence of a redox-active electronic conductor in the positive electrode of an all-solid lithium battery with a lithium metal negative electrode and a $LiFePO_4$ positive electrode. We demonstrate that P3HT is electroactive in the potential window of the charge/discharge cycle of the battery. This implies that two separate redox reactions occur in the positive electrode, one involving P3HT and the other involving $LiFePO_4$ (eqs 1 and 2). We assume that the $LiFePO_4$ redox reaction controls the electrode potential, which in turn dictates the $\sigma_{e,ox}$ of the P3HT-PEO block copolymer. In the open-circuit state, P3HT is in an electronically conducting state ($\sigma_{e,ox} = 10^{-3}$ S/cm), and $\sigma_{e,ox}$ increases to $10^{-2}$ S/cm during the charging step. This range of conductivities is significantly higher than the ionic conductivity of the P3HT-PEO block copolymer binder ($10^{-4}$ S/cm). This is important for enabling the redox reactions, as they involve equal moles of lithium ions and electronic charges (eqs 1 and 2). $\sigma_{e,ox}$ is above $10^{-4}$ S/cm for the majority of the discharge cycle, allowing for successful extraction of discharge capacity from the battery. However, at the tail end of the discharge cycle, $\sigma_{e,ox}$ decreases sharply to $10^{-7}$ S/cm; in this state the P3HT-PEO block copolymer binder is essentially an electronic insulator. This observation shows that the use of a semiconducting polymer such as P3HT as a conductive binder in a positive electrode provides an unprecedented route for overdischarge protection needed to prevent irreversible side reactions and safety failures in rechargeable batteries.

## EXPERIMENTAL METHODS

**Materials.** Ethynyl-terminated poly(3-hexylthiophene) (ethynyl-P3HT) was synthesized using Grignard metathesis polymerization.[42] Azide-terminated PEO (2000 g/mol, azide-PEO) was purchased from Polymer Source. Azide-PEO of 4200 g/mol was obtained through end-group functionalization of monomethoxy-PEO that was purchased from Polymer Source. Ethynyl-P3HT and azide-PEO were coupled using 1,3-dipolar cycloaddition click reaction to yield P3HT-PEO block copolymer (refer to ref 33 for more details on synthesis and purification). The molecular weight and regioregularity of ethynyl-P3HT were determined using $^1$H NMR. The polymers are characterized using a Viscotek autosampler, Viscotek triple detector (TDA 302), and a set of three Waters Styrogel HR columns (two HR3 and one HR4 column) with tetrahydrofuran (THF) as the mobile phase (flow rate of 1 mL/min, 35 °C). The GPC was calibrated using polystyrene standards. Table 1 lists the pertinent polymers used in this study. Polystyene-*block*-poly(ethylene oxide) (PS-PEO) was used as the polymer electrolyte separator. The $M_n$ of the PS block is 52.9 kg/mol, and $M_n$ of the PEO block is 67.6 g/mol. The volume fraction of PEO ($\phi_{EO}$) is 0.54.

**P3HT-PEO Block Copolymer Salt Sample.** All of the steps used to make the P3HT-PEO/LiTFSI mixtures were conducted in argon-filled gloveboxes (MBraun and Vacuum Atmospheres). LiTFSI was purchased from Novolyte and dried under vacuum at 120 °C for 3 days to remove any residual water. Neat P3HT-PEO samples were dried under vacuum at 90 °C for 2−3 days before making salt samples. LiTFSI/anhydrous-THF mixtures were prepared in a volumetric flask at a concentration of 0.5 g/mL. The P3HT-PEO samples were dissolved in anhydrous benzene at a concentration of 5 mg/mL in scintillation vials. Heating the sample slightly using a heated stir plate helped the dissolution process. An appropriate amount of LiTFSI/anhydrous-THF solution was added to the P3HT-PEO solution to obtain the desired salt concentration. The P3HT-PEO salt solutions were stirred overnight to ensure good mixing and placed in a custom-built airtight desiccator, which was transferred into a freeze-drying unit. The process ensured no exposure to air. We define $r_0$, the initial total salt concentration in the block copolymer, as the ratio between moles of LiTFSI and moles of EO units.

**Two-Terminal Conductivity Cell and Two-Terminal Electrochemical Cell.** Samples for conductivity measurements were prepared by hot pressing freeze-dried P3HT-PEO block copolymer with LiTFSI into a 125 $\mu$m thick Garolite G-10 spacer with an inner hole diameter of 3.88 mm. To assemble a two-terminal conductivity cell, nickel foil current collectors were pressed on both sides of the spacer at 90 °C. Nickel tabs were placed on both nickel foils. The sample was then sealed in aluminum-laminated pouch material (Showa Denko) using a vacuum sealer (Packing Aids Corp). To assemble the two-terminal electrochemical cell (Figure 1), we first measured the mass of the spacer before and after the addition of the polymer. A nickel foil current collector was pressed on one side of the spacer, while a piece of polymer electrolyte membrane approximately 3/16 in. in diameter (PS-PEO block copolymer with LiTFSI at $r_0 = 0.085$) was gently pressed on the other side of the spacer. A disk with a 3/16 in. diameter was punched from 150 $\mu$m thick lithium foil and was gently pressed on the other side of the polymer electrolyte membrane. Nickel tabs were placed on the lithium and on the nickel foil. The sample was then sealed in aluminum-laminated pouch material using a vacuum sealer. Samples were prepared and sealed in an argon-filled glovebox to ensure that the samples are air- and water-free.

**Three-Terminal Conductivity Cell and Three-Terminal Electrochemical Cell.** First, the P3HT-PEO/LiTFSI mixture was pressed into two eparate spacers at 90 °C. The mass of the spacer was recorded before and after the addition of the polymer. The thickness, $L$, of each polymer-filled spacer was measured (150−200 $\mu$m). Due to overfilling the spacer hole, the actual thickness is slightly larger than the spacer thickness, but is not an issue for taking measurements, as the polymer is a hard solid at 90 °C. Next, a piece of electroformed nickel mesh with a hole size of 344 $\mu$m and a wire width of 18.5 $\mu$m (Industrial Netting) was gently pressed between two spacers at 90 °C. This step needs to be done very carefully to ensure the mesh is not damaged and that the two polymer layers come into good contact to ensure negligible resistance at the interface. For the three-terminal conductivity cell (Figure 4a), nickel foil was gently pressed on both sides of the spacer. Nickel tabs were added to both the nickel foil electrodes and the nickel mesh electrodes. The sample was then sealed in aluminum-laminated pouch material using a vacuum sealer. In the case of the three-terminal electrochemical cell (Figure 3), a nickel foil electrode was gently pressed on one side of the spacer, while a piece of polymer electrolyte membrane was gently pressed on the other side of the spacer. A disk with 3/16 in. diameter was punched from 150 $\mu$m thick lithium foil and was gently pressed on the other side of the polymer electrolyte membrane. Nickel tabs were placed on the lithium, the nickel foil electrode, and the nickel mesh electrode. The sample was then sealed in aluminum-laminated pouch material using a vacuum sealer. Samples were

prepared and sealed in an argon-filled glovebox to ensure that the samples are air- and water-free.

**Galvanostatic Experiments.** Galvanostatic oxidation experiments were performed using a Bio-Logic VMP3 instrument and the Bio-Logic EC-Lab data acquisition software. A current density ($i$) of 0.17 mA/cm$^2$ is applied to the electrochemical cell for a specific amount of time ($t$). The oxidation level is denoted as $r_{ox}$, which is the ratio between the moles of electrons ($e^-$) removed to the moles of the 3-hexylthiophene moieties. The moles of $e^-$ removed is quantified using the following equation: moles $e^- = iAt/F$, where $A$ is the area of the sample (0.118 cm$^2$) and $F$ is Faraday's constant. The moles of $e^-$ removed equals the moles of $TFSI^-$ counterions needed to stabilize the holes generated. After reaching the desired $r_{ox}$ value, the cell is allowed to rest until the voltage begins to stabilize, as shown in Figure 2a. This value is taken as the equilibrium voltage ($E_{ox}$) corresponding to the desired $r_{ox}$ value.

**Conductivity Measurements Using Impedance Spectroscopy.** The impedance spectroscopy measurements were made using a Bio-Logics VMP3 instrument and Bio-Logics EC-Lab data acquisition software. The applied ac voltage was 50 mV with frequencies ranging from 1 MHz to 1 mHz. Resistances were calculated from the complex impedance data ($Z^* = Z' - iZ''$) where $Z'$ and $Z''$ are the real and imaginary impedances, respectively, using Nyquist plots ($-Z''$ *vs* $Z'$). The conductivity, $\sigma$, is given by

$$\sigma = \frac{L}{R} \tag{4}$$

where $L$ is the polymer thickness and $R$ is the resistance ($\Omega \cdot$cm$^2$), obtained from intersections of the Nyquist plots on the $Z'$ axis. All conductivity measurements were averaged over a minimum of three samples, and all reported error bars were calculated from one standard deviation. Physical arguments were used to arrive at a particular equivalent circuit. In all cases, we report the simplest equivalent circuit with the fewest elements that can describe the data. The Randomize + Simplex algorithm built into the EC-Lab software package was used to fit the impedance data.

**Scattering Experiments.** Small-angle X-ray scattering (SAXS) was taken at the Advanced Light Source (ALS) beamline 7.3.3 at Lawrence Berkeley National Lab. A silver behenate sample was used as a standard calibrant. The 2D scattering patterns were collected on a 1M Pilatus detector. The scattering patterns were reduced using the Nika macro for Igor Pro developed by Jan Ilavsky at Argonne National Laboratory.[43] The measured two-dimensional scattering data were averaged azimuthally to obtain intensity ($I$) *versus* magnitude of the scattering wave vector $q = 4\pi \sin(\theta/2)/\lambda$, where $\lambda$ is the wavelength of the incident X-rays (0.124 nm) and $\theta$ is the scattering angle.

*Conflict of Interest:* The authors declare no competing financial interest.

*Acknowledgment.* The measurement of electronic and ionic conductivities of the samples was supported by a grant from the National Science Foundation (CBET 0966632). The polymer synthesis was supported by the BATT program at Lawrence Berkeley National Laboratory, U.S. DOE Contract No. DE-AC02-05CH11231. SAXS experiments were performed at the Advanced Light Source, LBNL, a DOE national user facility supported by the DOE under the same contract. We gratefully acknowledge V. Srinivasan, T. Richardson, G. Chen, D. Hallinan, Jr., A. Teran, G. Stone, and S. Mullin for helpful discussions.

## REFERENCES AND NOTES

1. Yu, G.; Gao, J.; Hummelen, J. C.; Wudl, F.; Heeger, A. J. Polymer Photovoltaic Cells - Enhanced Efficiencies *via* a Network of Internal Donor-Acceptor Heterojunctions. *Science* **1995**, *270*, 1789–1791.
2. Steele, B. C. H.; Heinzel, A. Materials for Fuel-Cell Technologies. *Nature* **2001**, *414*, 345–352.
3. Tarascon, J. M.; Armand, M. Issues and Challenges Facing Rechargeable Lithium Batteries. *Nature* **2001**, *414*, 359–367.
4. Delacourt, C.; Laffont, L.; Bouchet, R.; Wurm, C.; Leriche, J. B.; Morcrette, M.; Tarascon, J. M.; Masquelier, C. Toward Understanding of Electrical Limitations (Electronic, Ionic) in $LiMPO_4$ (M = Fe, Mn) Electrode Materials. *J. Electrochem. Soc.* **2005**, *152*, A913–A921.
5. Matsen, M. W.; Bates, F. S. Unifying Weak- and Strong-Segregation Block Copolymer Theories. *Macromolecules* **1996**, *29*, 1091–1098.
6. Chen, T. A.; Wu, X. M.; Rieke, R. D. Regiocontrolled Synthesis of Poly(3-alkylthiophenes) Mediated by Rieke Zinc - Their Characterization and Solid-State Properties. *J. Am. Chem. Soc.* **1995**, *117*, 233–244.
7. Kuila, B. K.; Malik, S.; Batabyal, S. K.; Nandi, A. K. *In-Situ* Synthesis of Soluble Poly(3-hexylthiophene)/Multiwalled Carbon Nanotube Composite: Morphology, Structure, and Conductivity. *Macromolecules* **2007**, *40*, 278–287.
8. Liu, C.; Oshima, K.; Shimomura, M.; Miyauchi, S. Anisotropic Conductivity-Temperature Characteristic of Solution-Cast Poly(3-hexylthiophene) Films. *Synth. Met.* **2006**, *156*, 1362–1367.
9. Obrzut, J.; Page, K. A. Electrical Conductivity and Relaxation in Poly(3-hexylthiophene). *Phys. Rev. B* **2009**, *80*, 195211.
10. Bondarev, D.; Zednik, J.; Sloufova, I.; Sharf, A.; Prochazka, M.; Pfleger, J.; Vohlidal, J. Synthesis and Properties of Cationic Polyelectrolyte with Regioregular Polyalkylthiophene Backbone and Ionic-Liquid Like Side Groups. *J. Polym. Sci., Part A: Polym. Chem.* **2010**, *48*, 3073–3081.
11. Yim, K. H.; Whiting, G. L.; Murphy, C. E.; Halls, J. J. M.; Burroughes, J. H.; Friend, R. H.; Kim, J. S. Controlling Electrical Properties of Conjugated Polymers *via* a Solution-Based P-Type Doping. *Adv. Mater.* **2008**, *20*, 3319–3324.
12. Xuan, Y.; Liu, X.; Desbief, S.; Leclere, P.; Fahlman, M.; Lazzaroni, R.; Berggren, M.; Cornil, J.; Emin, D.; Crispin, X. Thermoelectric Properties of Conducting Polymers: The Case of Poly(3-hexylthiophene). *Phys. Rev. B* **2010**, 82.
13. MacDiarmid, A. G. "Synthetic Metals": A Novel Role for Organic Polymers (Nobel Lecture). *Angew. Chem., Int. Ed.* **2001**, *40*, 2581–2590.
14. Heeger, A. J. Semiconducting and Metallic Polymers: The Fourth Generation of Polymeric Materials (Nobel Lecture). *Angew. Chem., Int. Ed.* **2001**, *40*, 2591–2611.
15. Shirakawa, H. The Discovery of Polyacetylene Film: The Dawning of an Era of Conducting Polymers (Nobel Lecture). *Angew. Chem., Int. Ed.* **2001**, *40*, 2575–2580.
16. Chung, T. C.; Kaufman, J. H.; Heeger, A. J.; Wudl, F. Charge Storage in Doped Poly(thiophene) - Opitcal and Electrochemical Studies. *Phys. Rev. B* **1984**, *30*, 702–710.
17. Chiang, C. K.; Gau, S. C.; Fincher, C. R.; Park, Y. W.; Macdiarmid, A. G.; Heeger, A. J. Polyacetylene, (Ch)X - N-Type and P-Type Doping and Compensation. *Appl. Phys. Lett.* **1978**, *33*, 18–20.
18. Skotheim, T. A.; Reynolds, J. R. *Handbook of Conducting Polymers. Conjugated Polymers: Theory, Synthesis, Properties, and Characterization*, 3rd ed.; CRC Press: Boca Raton, FL, 2007.
19. Cho, J. H.; Lee, J.; Xia, Y.; Kim, B.; He, Y. Y.; Renn, M. J.; Lodge, T. P.; Frisbie, C. D. Printable Ion-Gel Gate Dielectrics for Low-Voltage Polymer Thin-Film Transistors on Plastic. *Nat. Mater.* **2008**, *7*, 900–906.
20. Panzer, M. J.; Frisbie, C. D. Exploiting Ionic Coupling in Electronic Devices: Electrolyte-Gated Organic Field-Effect Transistors. *Adv. Mater.* **2008**, *20*, 3177–3180.
21. Larsson, O.; Laiho, A.; Schmickler, W.; Berggren, M.; Crispin, X. Controlling the Dimensionality of Charge Transport in an Organic Electrochemical Transistor by Capacitive Coupling. *Adv. Mater.* **2011**, *23*, 4764–4769.
22. Bubnova, O.; Berggren, M.; Crispin, X. Tuning the Thermoelectric Properties of Conducting Polymers in an Electrochemical Transistor. *J. Am. Chem. Soc.* **2012**, *134*, 16456–16459.
23. Macinnes, D.; Druy, M. A.; Nigrey, P. J.; Nairns, D. P.; Macdiarmid, A. G.; Heeger, A. J. Organic Batteries - Reversible *N*- and *P*-Type Electrochemical Doping of Polyacetylene, $(CH)_x$. *J. Chem. Soc., Chem. Commun.* **1981**, 317–319.

24. Kaufman, J. H.; Chung, T. C.; Heeger, A. J.; Wudl, F. Poly-(thiophene) - a Stable Polymer Cathode Material. *J. Electrochem. Soc.* **1984**, *131*, 2092–2093.
25. Novak, P.; Muller, K.; Santhanam, K. S. V.; Haas, O. Electrochemically Active Polymers for Rechargeable Batteries. *Chem. Rev.* **1997**, *97*, 207–281.
26. Mike, J. F.; Lutkenhaus, J. L. Recent Advances in Conjugated Polymer Energy Storage. *J. Polym. Sci., Part B: Polym. Phys.* **2013**, *51*, 468–480.
27. Chen, G. Y.; Thomas-Alyea, K. E.; Newman, J.; Richardson, T. J. Characterization of an Electroactive Polymer for Overcharge Protection in Secondary Lithium Batteries. *Electrochim. Acta* **2005**, *50*, 4666–4673.
28. Chen, G. Y.; Richardson, T. J. Overcharge Protection for High Voltage Lithium Cells Using Two Electroactive Polymers. *Electrochem. Solid-State Lett.* **2006**, *9*, A24–A26.
29. Guoying, C.; Richardson, T. J. Overcharge Protection for Rechargeable Lithium Batteries Using Electroactive Polymers. *Electrochem. Solid-State Lett.* **2004**, *7*, A23–A26.
30. Patel, S. N.; Javier, A. E.; Stone, G. M.; Mullin, S. A.; Balsara, N. P. Simultaneous Conduction of Electronic Charge and Lithium Ions in Block Copolymers. *ACS Nano* **2012**, *6*, 1589–1600.
31. Yang, X.; Loos, J.; Veenstra, S.; Verhees, W.; Wienk, M.; Kroon, J.; Michels, M.; Janssen, R. Nanoscale Morphology of High-Performance Polymer Solar Cells. *Nano Lett.* **2005**, *5*, 579–583.
32. Eitouni, H. B.; Balsara, N. P. Thermodynamics of Polymer Blends. In *Physical Properties of Polymers Handbook*; Mark, J. E., Ed.; Springer: New York, 2007; pp 339−356.
33. Javier, A. E.; Patel, S. N.; Hallinan, D. T.; Srinivasan, V.; Balsara, N. P. Simultaneous Electronic and Ionic Conduction in a Block Copolymer: Application in Lithium Battery Electrodes. *Angew. Chem., Int. Ed.* **2011**, *50*, 9848–9851.
34. Stafstrom, S.; Bredas, J. L. Evolution of the Electronic-Structure of Polyacetylene and Polythiophene As a Function of Doping Level and Lattice Conformation. *Phys. Rev. B* **1988**, *38*, 4180–4191.
35. Yuan, R.; Teran, A. A.; Gurevitch, I.; Mullin, S. A.; Wanakule, N. S.; Balsara, N. P. Ionic Conductivity of Low Molecular Weight Block Copolymer Electrolytes. *Macromolecules* **2013**, *46*, 914–921.
36. Bredas, J. L.; Themans, B.; Fripiat, J. G.; Andre, J. M.; Chance, R. R. Highly Conducting Polyparaphenylene, Polypyrrole, and Polythiophene Chains - an *Ab Initio* Study of the Geometry and Electronic-Structure Modifications Upon Doping. *Phys. Rev. B* **1984**, *29*, 6761–6773.
37. Ciprelli, J. L.; Clarisse, C.; Delabouglise, D. Enhanced Stability of Conducting Poly(3-Octylthiophene) Thin Films Using Organic Nitrosyl Compounds. *Synth. Met.* **1995**, *74*, 217–222.
38. Jiang, X.; Harima, Y.; Yamashita, K.; Tada, Y.; Ohshita, J.; Kunai, A. Doping-Induced Change of Carrier Mobilities in Poly(3-hexylthiophene) Films with Different Stacking Structures. *Chem. Phys. Lett.* **2002**, *364*, 616–620.
39. Shimotani, H.; Diguet, G.; Iwasa, Y. Direct Comparison of Field-Effect and Electrochemical Doping in Regioregular Poly(3-hexylthiophene). *Appl. Phys. Lett.* **2005**, *86*.
40. Arkhipov, V. I.; Emelianova, E. V.; Heremans, P.; Bassler, H. Analytic Model of Carrier Mobility in Doped Disordered Organic Semiconductors. *Phys. Rev. B* **2005**, *72*, 235202.
41. Richardson, T. J.; Ross, P. N. Overcharge Protection for Rechargeable Lithium Polymer Electrolyte Batteries. *J. Electrochem. Soc.* **1996**, *143*, 3992–3996.
42. Jeffries-El, M.; Sauve, G.; McCullough, R. D. *In-Situ* End-Group Functionalization of Regioregular Poly(3-alkylthiophene) Using the Grignard Metathesis Polymerization Method. *Adv. Mater.* **2004**, *16*, 1017–1019.
43. Ilavsky, J. Nika: Software for Two-Dimensional Data Reduction. *J. Appl. Crystallogr.* **2012**, *45*, 324–328.